Electrical Power and Energy Systems 135 (2022) 107453

Contents lists available at ScienceDirect

International Journal of Electrical Power and Energy Systems

journal homepage: www.elsevier.com/locate/ijepes

Dynamic analysis of variable-speed pumped storage plants for mitigating effects of excess wind power generation

Yuwen Deng [a,b], Pengfei Wang [a,b], Alessandro Morabito [c], Wenfeng Feng [a], Apel Mahmud [d], Diyi Chen [a,b,*], Patrick Hendrick [c]

[a] Institute of Water Resources and Hydropower Research, Northwest A&F University, Yangling 712100, Shaanxi, PR China
[b] Key Laboratory of Agriculture Soil and Water Engineering in Arid and Semiarid Areas, Ministry of Education, North A&F University, Yangling 712100, Shaanxi, PR China
[c] Aero-Thermo-Mechanics Department, Université libre de Bruxelles, Brussels 1050, Belgium
[d] Electrical Power and Energy Systems Research Lab, School of Engineering, Deakin University, Geelong, VIC 3216, Australia

ARTICLE INFO

Keywords:
Variable-speed pumped storage plant
Power storage regulation
Wind power variation
Numerical model

ABSTRACT

The integration of hydropower and variable energy sources emerges as a functional method for handling power variability. Due to the advantage of adjustable power input of the pumped storage operation, variable-speed pumped storage plants (VSPSPs) have been proposed as a potential alternative to traditional fixed-speed pumped storage plants (FSPSPs) for dealing with the variable storage demand. The performance evaluation of VSPSPs in coping with changes in loads and variations in renewable energy sources during the energy storage process is crucial to ensure adequate flexibility and reliability of the grid. In this paper, the regulation performance assessment of VSPSP in mitigating wind power variations is presented based on IEEE 14-bus test system. The goal is to draw up the regulation reliability of the VSPSP under pumping mode for balancing the dynamic characteristics of wind power. Specifically, a numerical model of VSPSPs with doubly-fed induction machines is described and developed which is then validated by the measured data in the form of a case study. Moreover, by considering ten wind scenarios having differences in frequency, gradient, guts intensity, and standard deviation; simulations of VSPSP performing power regulation in the pump mode are conducted and the dynamic regulation effects are assessed. Finally, the power regulation quality comparison is provided between the power generation and storage modes to validate the regulation reliability of the VSPSP under the pumped storage operation. The regulation time delay (RTD) ratios of VSUs to FSUs are found in the range of 4.67–9.16%, demonstrating the rapidity of VSPSPs in the power regulation.

1. Introduction

The penetration of intermittent renewable energy sources (IRESs), e.g. wind and solar into power grids is constantly growing and balancing the power injections from IRESs is a crucial topic in the energy industry all over the world [1]. Due to the flexible and rapid power adjustment of the hydraulic machinery [2,3], conventional hydropower plants and pumped storage systems have traditionally been undertaking a large portion of the regulation task in many power systems [4-6]. Research and implementation for the joint operation of hydro and IRESs have become more common, such as in hydro-wind [7,8], hydro-photovoltaic (PV) [9,10], and hydro-PV-wind [11,12] hybrid power systems.

The operational mechanisms of storage and generation of pumped storage plants (PSPs) (as illustrated in Fig. 1) add significant advantages in increasing the economic benefits and availability of IRESs [4,5]. Specifically, the phenomenon of excess power generation commonly occurs in the electricity production peak phases of IRESs [13,14]. The combined operation with PSPs enables the energy that exceeds the instant demand to be stored instead of cutrtailing. The reserve of energy can be used for tackling power shortages during load peak periods [3,15,16]. For this reason, recently, the excellent complementarity with PSPs promotes IRESs to be combined with hydro-equipment [8]. Nevertheless, the widely implemented fixed-speed pumped storage plants (FSPSPs) cannot regulate power flows under pumping operations due to their rigid operating characteristics [17,18]. In this case, the pumping system cannot continuously afford the duty of mitigating the power variation which may extremely influence the reliability of the

* Corresponding author at: Institute of Water Resources and Hydropower Research, Northwest A&F University, Yangling 712100, Shaanxi, PR China.
E-mail address: diyichen@nwsuaf.edu.cn (D. Chen).

https://doi.org/10.1016/j.ijepes.2021.107453
Received 8 October 2020; Received in revised form 31 May 2021; Accepted 24 July 2021
Available online 3 September 2021

Nomenclature

Acronyms

DFIM	Doubly-Fed Induction Machine
FSFC	Full Size Frequency Converter
FSPSP	Fixed-Speed Pumped Storage Plant
FSU	Fixed-Speed Unit
GSC	Grid Side Convertor
ORS	Optimum Rotor Speed
OGVO	Optimum Guide Vane Opening
RBIM	Radial Basis Interpolation Method
RSC	Rotor Side Convertor
RTD	Regulation Time Delay
VRE	Variable Renewable Energy
VSPSP	Variable-Speed Pumped Storage Plant
VSU	Variable-Speed Unit
WF	Wind Farm

Constants

α	constant term of difference equation (pu.)
β	constant term of difference equation (pu.)
ρ	water density (kg/m^3)
a	interpolation coefficient (pu.)
b	interpolation coefficient (pu.)
C	DC bus capacity (F)
D	the diameter of penstock (m)
D_t	damping constant (pu.)
$e_{m\omega,y,h}$	partial derivative coefficient (pu.)
$e_{q\omega,y,h}$	partial derivative coefficient (pu.)
f	friction resistance coefficient (m/s^2)
g	gravity acceleration (m/s^2)
h_w	pipeline characteristic coefficient (pu.)
L_g	grid inductance (H)
L_m	magnetizing inductance (H)
L_r	rotor inductance (H)
L_s	stator inductance (H)
p	pole pair number (pu.)
R_g	grid resistance (Ω)
R_r	rotor resistance (Ω)
R_s	stator resistance (Ω)
T_a	mechanical time constant (s)
T_r	elastic water hammer time constant (s)
T_w	water starting time constant (s)
T_y	servo time constant (s)

Subscripts, Superscripts

d	d-axis component
i	iteration number between 1 and N
j	iteration number between 1 and N
q	q-axis component
ref	reference value

Variables

Ω_r	mechanical rotor speed (rpm)
μ	angle between penstock and horizontal (°)
η	pump mode operational efficiency (%)
ω_r	rotor frequency (rad/s)
ω_s	stator frequency (rad/s)
ω_g	grid frequency (rad/s)
h	pump water head (m)
H_s	static water head (m)
i_g	grid current (A)
i_{load}	DC side load current (A)
i_r	rotor current (A)
i_s	stator current (A)
P_m	Pump-turbine mechanical power (N·m/s)
P_{in}	VSPSP power input (MW)
q	pump flow rate (m^3/s)
S	switching function (pu.)
T_e	electromagnetic torque (N·m)
T_m	motor torque (N·m)
U_{dc}	DC bus voltage (V)
u_g	grid voltage (V)
u_r	rotor voltage (V)
u_s	stator voltage (V)
v	flow velocity (m/s)
v_g	AC side voltage of converter (V)
x	penstock direction displacement (m)
y	guide vane opening (%)

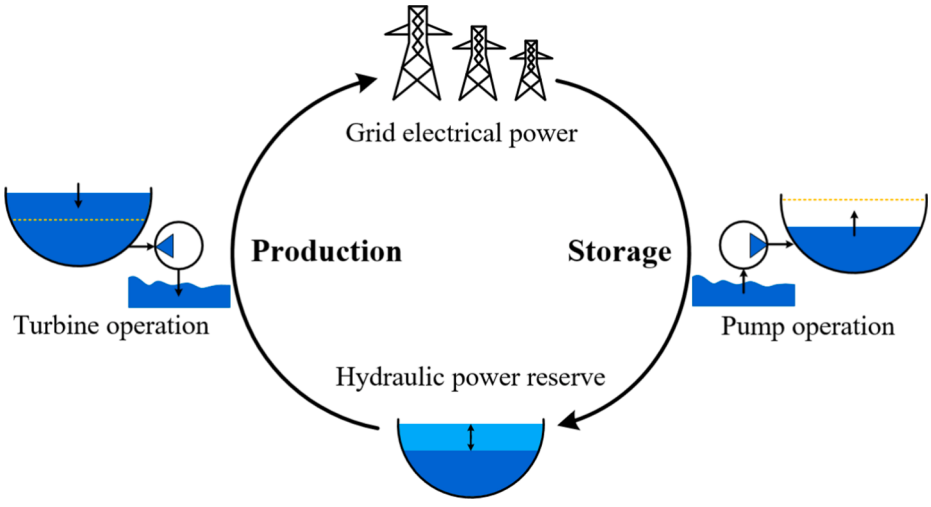

Fig. 1. The operating principle of PSPs: storage (pump operation) and production (turbine operation).

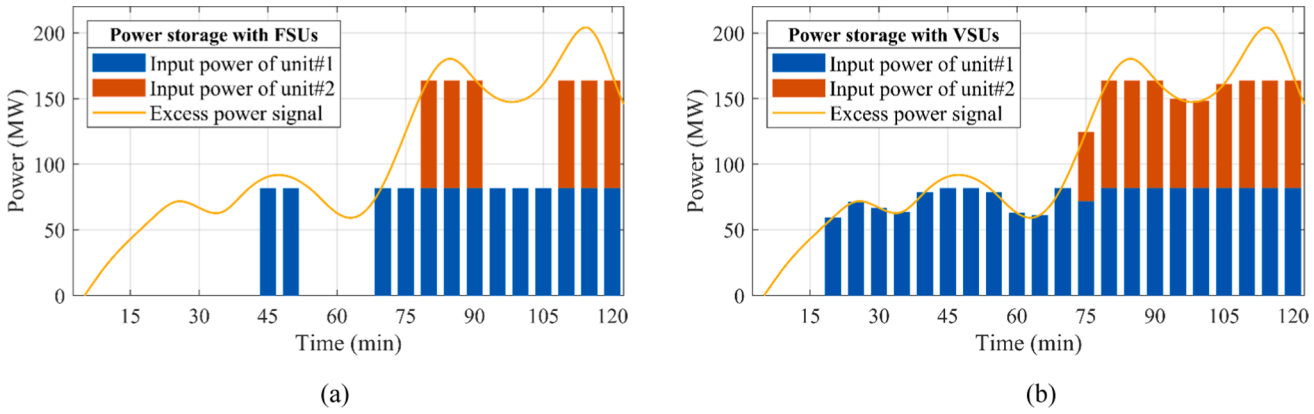

Fig. 2. Results of the field test in a Japanese VSPSP: (a) Power storage with FSUs; (b) Power storage with VSUs. (The power input adjustable range of the VSUs is 53–82 MW [26].)

Table 1
Comparison of previous research and this paper in the field of integrating PSPs with wind farms.

Previous research		Reference No.
Study time scale	Operation state of PSP	
Equal to or Larger than minute	Power generation	[5,7,8,16]
	Pumped storage	[5,8,16]
Second	Power generation	[24,30,31]
	Pumped storage	/
This paper		/
Study time scale	Operation state of PSP	
Second	Pumped storage	

power supply for the IRES-PSPs hybrid power system.

Recently, an advanced hydropower technology, variable-speed (or adjustable-speed) pumped storage plants (VSPSPs), has become a new research orientation [19-23] due to its several advantages compared to traditional FSPSPs where these advantages include the rapidity, high efficiency, and reliability in operation and regulation [24]. Among the various benefits of a VSPSP, the most significant and indispensable one is its flexible operation in the pumped storage mode [25], benefiting from the adjustable input power. In general, the minimum power input is accounting for about 50–70% of the rated power [26]. A comparison of the power storage performance of variable-speed units (VSUs) and fixed-speed units (FSUs) were made in a Japanese VSPSP and the results are shown in Fig. 2, underling the operational advantages of VSUs in the pumping mode in terms of the flexibility and load factor.

The adjustable power input enables the VSPSP to effectively compensate to the storage load variation. Consequently, regarding PSPs, the replacement from the FSUs to variable- VSUs may extremely ameliorate the power storage performance and exceedingly extend the time for the power regulation. The study of whether the VSUs can cope with the power variation of IRESs or not is of great significance which is directly relevant to the stability and reliability of the power supply for the IRESs-PSPs hybrid energy system.

Among the abovementioned features of VSUs, this work focuses on the power storage regulation performance of VSPSPs in handling the wind power variations which is of great significance to the promotion of the multi-renewable energy system. On this topic, the literature provides research activities on the dynamic behaviors of VSPSPs in the power regulation as on the 400 MW VSUs of Ohkawachi PSP case study [25]. The design principle and control theory of the case study for VSUs were expounded in both generation and storage modes as the time response of power adjustment was measured and analyzed [25]. A mathematical model was developed and simulation results were compared with the real measured data in [26]. The dynamic simulation of VSPSPs with doubly-fed induction machines (DFIMs) was carried out and simulation results for grid-connected operations with three-phase short circuits were provided in [27,28]. The mathematical model for VSPSPs was developed and a caparative study for analyzing the dynamic behaviors of VSUs and FSUs was presented in [24]. Regarding the integration of PSPs with IRESs, especially for wind energy, several studies have been conducted. An investigation on alayzing the benefit of FSPSPs for optimally integrating the wind power in Kenya was developed in [5] based on an hour-scale and a control approach is proposed for optimizing the combined operation. The utilization of VSPSPs for balancing power fluctuations generated by the wind power in an isolated grid was achieved in [29]. Different control strategies for the speed control loop of a VSU in an isolated power system were analyzed and compared based on scenarios with wind power variations [30]. A regulation performance assessment during generating mode of VSUs for mitigating the wind power variations was developed in [24] and the assessment results were compared with FSUs.

In this context, this paper engages two crucial aspects of VSPSPs:

(1) Previous studies for integrating PSPs with wind farms available in the literature are often focused on the joint operation based on timescales larger than an hour [5,7,8,16]. Refining the analysis at the timescale of seconds is could bring novel perspectives and expand the current understanding of the system. Therefore, this research investigates the dynamic behaviors of VSUs to analyze operational stabilities during power fluctuations in the pumping mode on multi-timescales by an extended mathematical model; and
(2) Moreover, this paper evaluates the regulation quality of VSPSPs in the pumped storage mode, especially during the process of handling wind power variations. The research activity on the dynamic behaviors and regulation performance of VSPSPs in pumping mode is indeed relatively a new area, especially in the process of mitigating the wind power variation: a large number of published work focus on the generation mode [24,30,31] (see Table 1).

The content of this paper can be organized as follows. In Section 2, a comprehensive mathematical model of VSUs depicting the pumping mode in the grid-connected condition is developed. In Section 3, the control system of VSUs in the pumped-storage mode is studied. In Section 4, the modeling is validated through a comparison with on-site measurement data. A test system is modeled based on IEEE bus system and the simulation results of VSUs mitigating the excess wind power are presented in Section 5 by considering different wind profile scenarios. In Section 6, a regulation quality comparison is introduced to compare the regulation performance of the generation mode and storage mode.

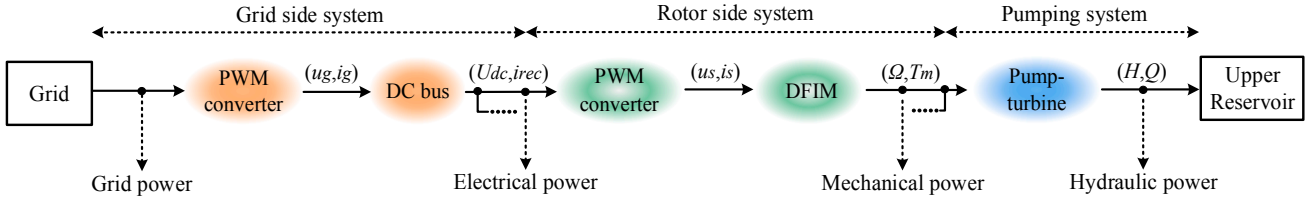

Fig. 3. Block diagram representation for the energy conversion system of VSPSPs in the pumped storage mode [34].

2. Mathematical modelling of VSPSPs under the pumped storage operation

In this section, the dynamic modeling of VSPSPs in the pumped storage mode is developed for the grid-connected condition. The focus of this work is on the performance of the power storage regulation for which the set-point of active power input of the system is important for the case studies in the following sections.

According to the distinct energy conversion processes, VSPSPs can be generally divided into three subsystems defining the power storage mechanism via VSUs. Following the representation in Fig. 3, one can find the grid-side system, rotor-side system, and pumping system. The hydraulic-mechanical–electrical integrated model of VSPSPs is presented in the following subsections.

2.1. Grid side system modelling

The grid-side system includes a pulse width modulated (PWM) converter and a DC-bus which ensures the connection between the grid and DFIM. The grid-side generation system can be considered as a three-phase high-voltage source with a grid impedance (including grid resistance (R_g) and grid inductance (L_g)) and a low voltage transformer. The modeling of the grid-side system in the *dq* reference frame can be developed as indicated in Eqs. (1) and (2)

$$\mathrm{u}_{gd} = R_g i_{gd} + L_g \frac{di_{gd}}{dt} - \omega_g L_g i_{gq} + \mathrm{v}_{gd}, \tag{1}$$

$$\mathrm{u}_{gq} = R_g i_{gq} + L_g \frac{di_{gq}}{dt} + \omega_g L_g i_{gd} + \mathrm{v}_{gq}. \tag{2}$$

Here, the PWM converter and DC-bus are modeled according to Eqs. (3) and (4)

$$\mathrm{i}_{rec} = \frac{3}{2}\left(S_d i_{gd} + S_q i_{gq}\right), \tag{3}$$

$$C\frac{\mathrm{d}U_{dc}}{dt} = \mathrm{i}_{rec} - i_{\mathrm{load}}. \tag{4}$$

2.2. Rotor side system modelling

Compared with conventional FSUs, the chief operating difference of VSUs lays in the electrical-subsystem, where DFIM replaces the synchronous electric machinery. Eq. (5) describes the frequency slip function, presenting the VSUs operating principle

$$\omega_{\mathrm{slip}} = \omega_s - \omega_r. \tag{5}$$

The relation between the rotor angular frequency and the mechanical rotational speed of the rotor can be written as

$$\omega_{\mathrm{r}} = p\Omega_{\mathrm{r}}. \tag{6}$$

The state-space representation in the *d-q* reference frame is adopted for the dynamic DFIM model as presented in [24,26-28] and shown in Eqs. (7)–(10)

$$\frac{\mathrm{d}I}{dt} = AI + BU \tag{7}$$

where

$$I = [i_{sd}\ i_{sq}\ i_{rd}\ i_{rq}]^T,\ \mathrm{U} = [\mathrm{u}_{sd}\ \mathrm{u}_{sq}\ \mathrm{u}_{rd}\ \mathrm{u}_{rq}]^T, \tag{8}$$

$$A = \left(\frac{1}{\sigma L_s L_r}\right)\begin{pmatrix} -R_s L_r & \omega_r L_m^2 + \omega_s \sigma L_s L_r & R_r L_m & \omega_r L_m L_r \\ -\omega_r L_m^2 - \omega_s \sigma L_s L_r & -R_s L_r & -\omega_r L_m L_r & R_r L_m \\ R_s L_m & -\omega_r L_m L_s & -R_r L_s & -\omega_r L_s L_r + \omega_s \sigma L_s L_r \\ \omega_r L_m L_s & R_s L_m & \omega_r L_s L_r - \omega_s \sigma L_s L_r & -R_r L_s \end{pmatrix}, \tag{9}$$

$$B = \left(\frac{1}{\sigma L_s L_r}\right)\begin{pmatrix} L_r & 0 & -L_m & 0 \\ 0 & L_r & 0 & -L_m \\ -L_m & 0 & L_s & 0 \\ 0 & -L_m & 0 & L_s \end{pmatrix}, \tag{10}$$

$$\sigma = 1 - \frac{L_m^2}{L_s L_r}. \tag{11}$$

The active *P* and reactive power *Q* can be described through Eq. (12)

$$\begin{cases} P = -\frac{3}{2}\omega_s L_m\left(i_{sq}i_{rd} - i_{sd}i_{rq}\right) + \frac{3}{2}\omega_{slip}L_m\left(i_{sq}i_{rd} - i_{sd}i_{rq}\right) = -\frac{3}{2}\omega_r L_m\left(i_{sq}i_{rd} - i_{sd}i_{rq}\right) \\ Q = -\frac{3}{2}\omega_s L_m\left(-i_{sq}i_{rd} - i_{sd}i_{rq}\right) + \frac{3}{2}\omega_{slip}L_m\left(i_{sq}i_{rd} + i_{sd}i_{rq}\right) = \frac{3}{2}\left(\omega_{\text{slip}} + \omega_s\right)L_m\left(i_{sq}i_{rd} - i_{sd}i_{rq}\right) \end{cases} \tag{12}$$

And the electromagnetic torque of generator-motor can be expressed as

$$T_{\text{e}} = \frac{3}{2}\text{p}L_m\left(i_{\text{sq}}i_{rd} - i_{sd}i_{rq}\right) \tag{13}$$

Considering the damping term, the swing equation of the DFIM can be described as [24,32]

$$T_{\text{a}}\frac{\text{d}\Omega_{\text{r}}}{dt} = \frac{T_a}{\text{p}}\frac{\text{d}\omega_{\text{r}}}{dt} = T_m - T_e - D_t\omega_{\text{r}}. \tag{14}$$

It can be inferred from Eqs. (13) and (14) that the DFIM can regulate the rotor speed through altering the current, which is the rotor speed control strategy in the pumped storage mode.

2.3. Pumping system modelling

The pumping system includes two major sub-systems such as the elastic penstock and pump turbine. The dynamic modeling of these components are provided in the following subsections.

2.3.1. Elastic penstock modelling

In general, the flow characteristic in the penstock is described by the partial differential equations of the motion equation and continuity equations [32], as shown in Eq. (15)

$$\begin{cases} \text{g}\frac{\partial \text{h}}{\partial x} + \frac{\partial v}{\partial t} + v\frac{\partial v}{\partial t} + \frac{fv|v|}{2D} = 0 \\ \frac{\partial h}{\partial t} + v\frac{\partial h}{\partial x} + \frac{a^2}{g}\frac{\partial v}{\partial x} + v\sin\alpha = 0 \end{cases} \tag{15}$$

The transfer function of the penstock considering the elastic water-hammer can be expressed as

$$G_{\text{h}}(s) = -2h_w\frac{\frac{1}{48}T_r^3 s^3 + \frac{1}{2}T_r s}{\frac{1}{8}T_r^2 s^2 + 1}. \tag{16}$$

2.3.2. Pump-turbine modelling

Pump-turbine units in pumping mode act as hydraulic pumps and these are powered by the mechanical energy to convey a water flow between two reservoirs at different heads. The mechanical power Pm can be described in Eq. (17)

$$P_{\text{m}} = \eta\rho g\text{qh}. \tag{17}$$

A linearized pump-turbine model with six coefficients is generally applied to describe the pump-turbine characteristics [24,32], as shown in Eq. (18)

$$\begin{cases} \text{T}_{\text{m}} = e_{my}y + e_{m\omega}\omega_r + e_{mh}h \\ q = e_{qy}y + e_{q\omega}\omega_r + e_{qh}h \end{cases} \tag{18}$$

3. Hierarchy of the control system for VSPSPs

The VSUs have diverse control structures as shown in Fig. 4 [33]. When a power regulation command signal is received, the optimizer of VSUs reacting initially to calculate the optimum references set points of the rotor speed (ω_{rref}) and guide vane opening (y_{ref}). Then, optimal reference set points are communicated to each controller and these controllers start to adjust theselves for achieving the power regulation task. The control strategies and optimization calculation approach are studied in details and discussed in this section.

3.1. Optimal reference profiles for the rotor speed and guide vane opening

Variable-speed pump-turbine units normally optimize the rotor speed and guide vane opening to maximize the operational efficiency at given power references in both turbine and pump modes [24-28]. The input power of the system and static water head are the decisive factors for the calculation of optimal values in VSUs which are discussed in [24,28] and these can be presented as shown in Fig. 5.

Generally speaking, the references measured by the experiment are limited [25] and mathematical approaches are necessary for forecasting those optimum references beyond the measurement data. Recently, constructing fitting functions and adopting interpolation approaches are widely applied in data prediction of energy conversion equipment [31,33,34]. A radial basis interpolation method (RBIM) based on the operational data of a variable-speed pump-turbine unit (VSPTU) with high accuracy is applied in this work to make the simulation results more consistent with the situations in real-time operation. The bivariate inverse quadratic function of RBIM can be described as

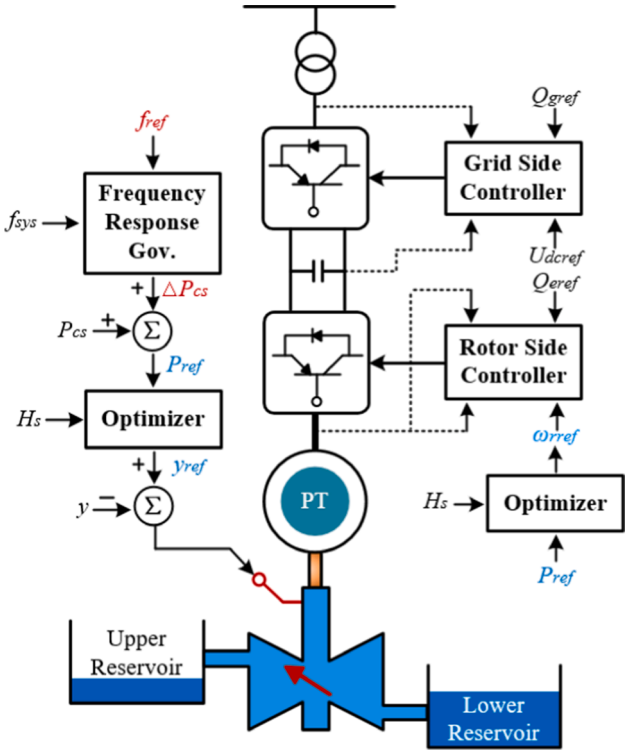

Fig. 4. The control structure of VSUs in the pumped storage mode [33]. During the regulation process for mitigating the variation of IRESs, the main adjustment objects are described in blue: active power (P_{ref}), guide vane opening (y_{ref}), and rotor speed (ω_{rref}).

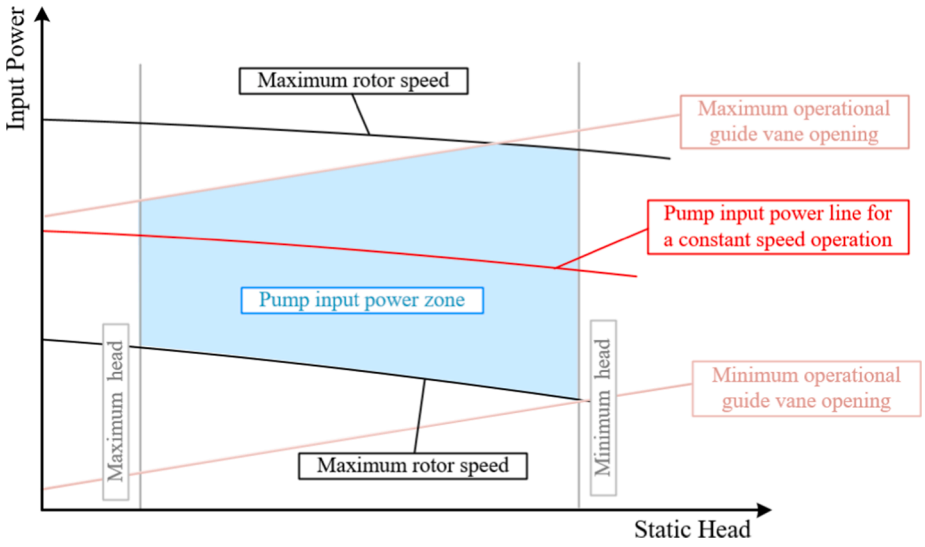

Fig. 5. Optimal reference data curves of VSU under pumped storage operation-projection on system input versus static head axis.

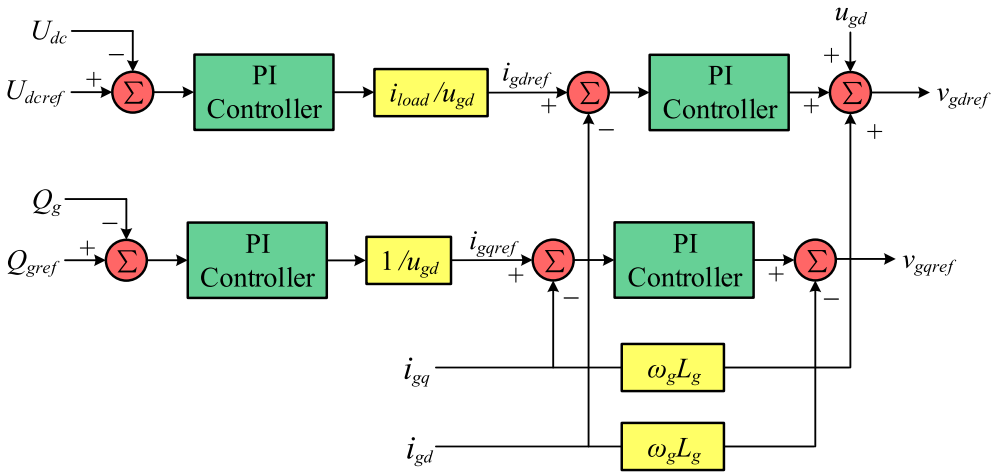

Fig. 6. The vector control structure of VSUs for the grid-side converter.

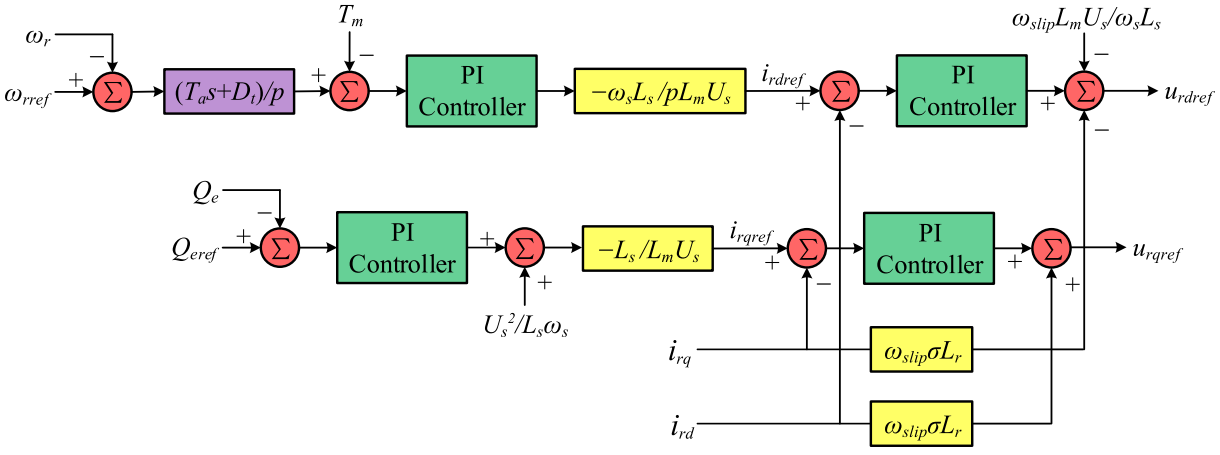

Fig. 7. The vector control structure of VSUs for the rotor-side converter.

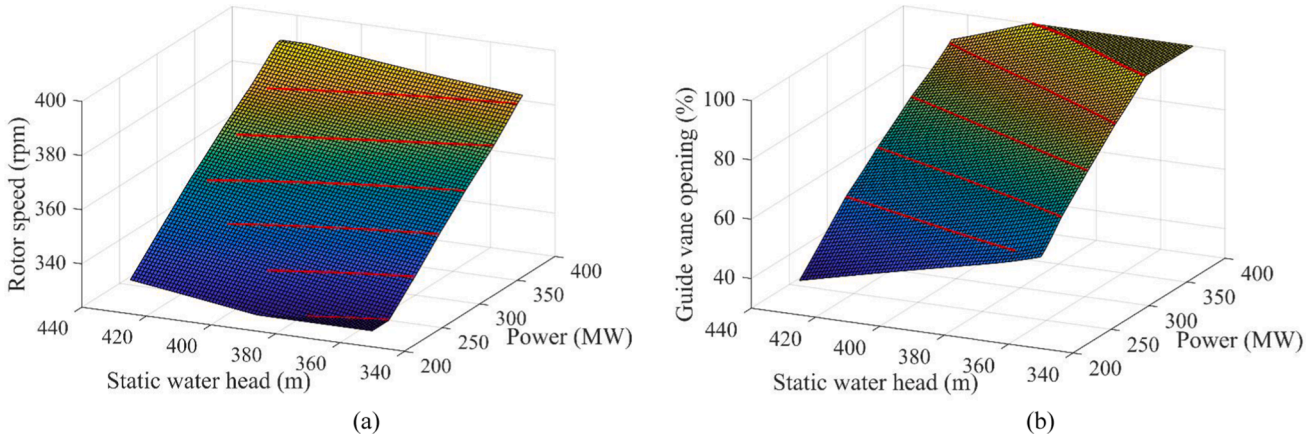

Fig. 8. Interpolation results of optimum references: (a) rotor speed; (b) guide vane opening.

Table 2
Comparisons of the interpolation result and on-site measurements.

Power signal and state	ORS		OGVO	
	Measurementdata (rpm)	Interpolation result (rpm)	Measurement data (%)	Interpolation result (%)
Initial state of RPS (246 MW)	347.4	347.32	65.6	65.54
Completion state of RPS (400 MW)	366.0	366.02	82.6	82.64
Initial state of SPS (246 MW)	347.4	347. 32	65.6	65.54
Completion state of SPS (324 MW)	385.7	385.66	96.8	96.83

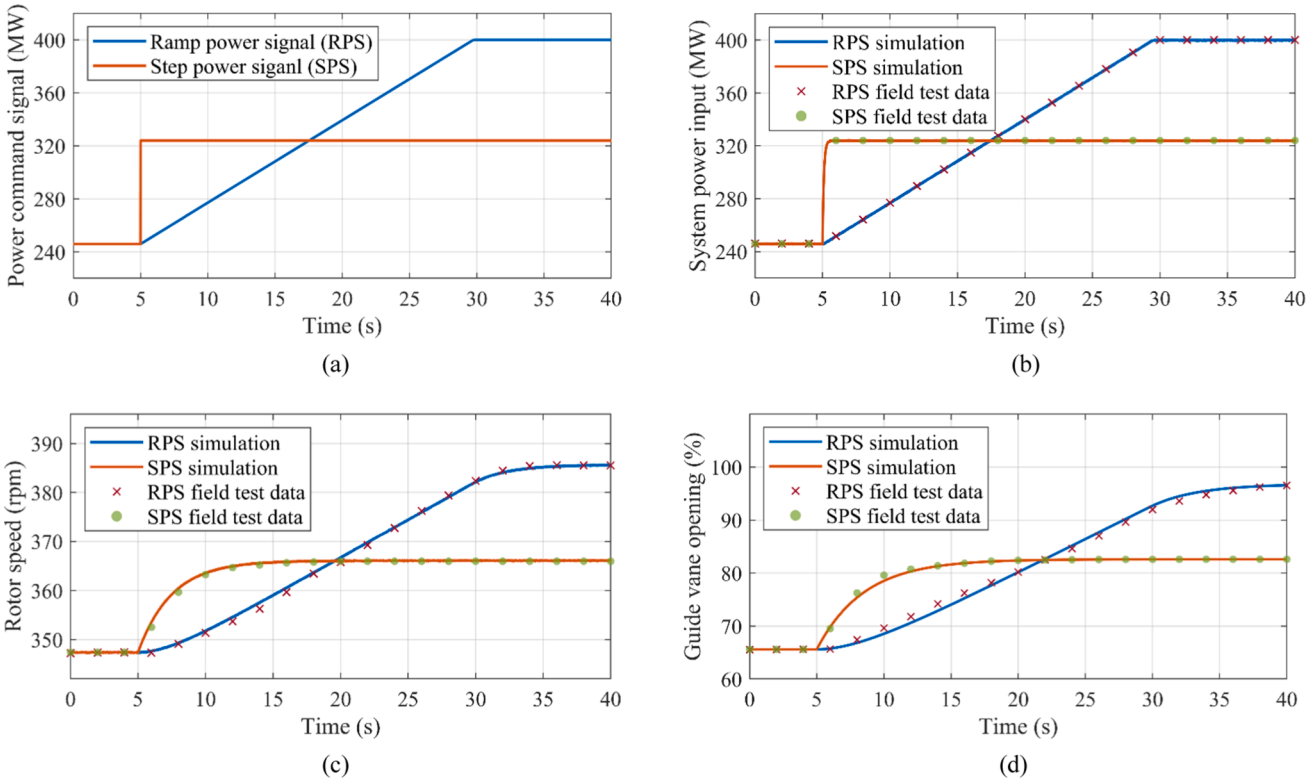

Fig. 9. A comparison of field test data and simulation results: (a) power command signal; (b) system input power; (c) rotor speed; (d) guide vane opening.

$$\omega_{\mathrm{rref}} = f_1(\mathrm{H}_s, P_{in}) = \sum_{\mathrm{i}=1}^{n} a_i \left[(H_s - H_{s_i})^2 + (P_{in} - P_{in_i})^2 + \alpha \right]^{\frac{1}{2}}, \tag{19}$$

$$y_{\mathrm{ref}} = f_2(\mathrm{H}_s, P_{in}) = \sum_{j=1}^{n} b_j \left[\left(H_s - H_{s_j}\right)^2 + \left(P_{in} - P_{in_j}\right)^2 + \beta \right]^{\frac{1}{2}}. \tag{20}$$

3.2. Control strategy for the guide vane system

Guide vanes generally regulate the water flow intensity and directions in the power generation mode [24]. The same system in the power storage mode adjusts the guide vane opening for matching the

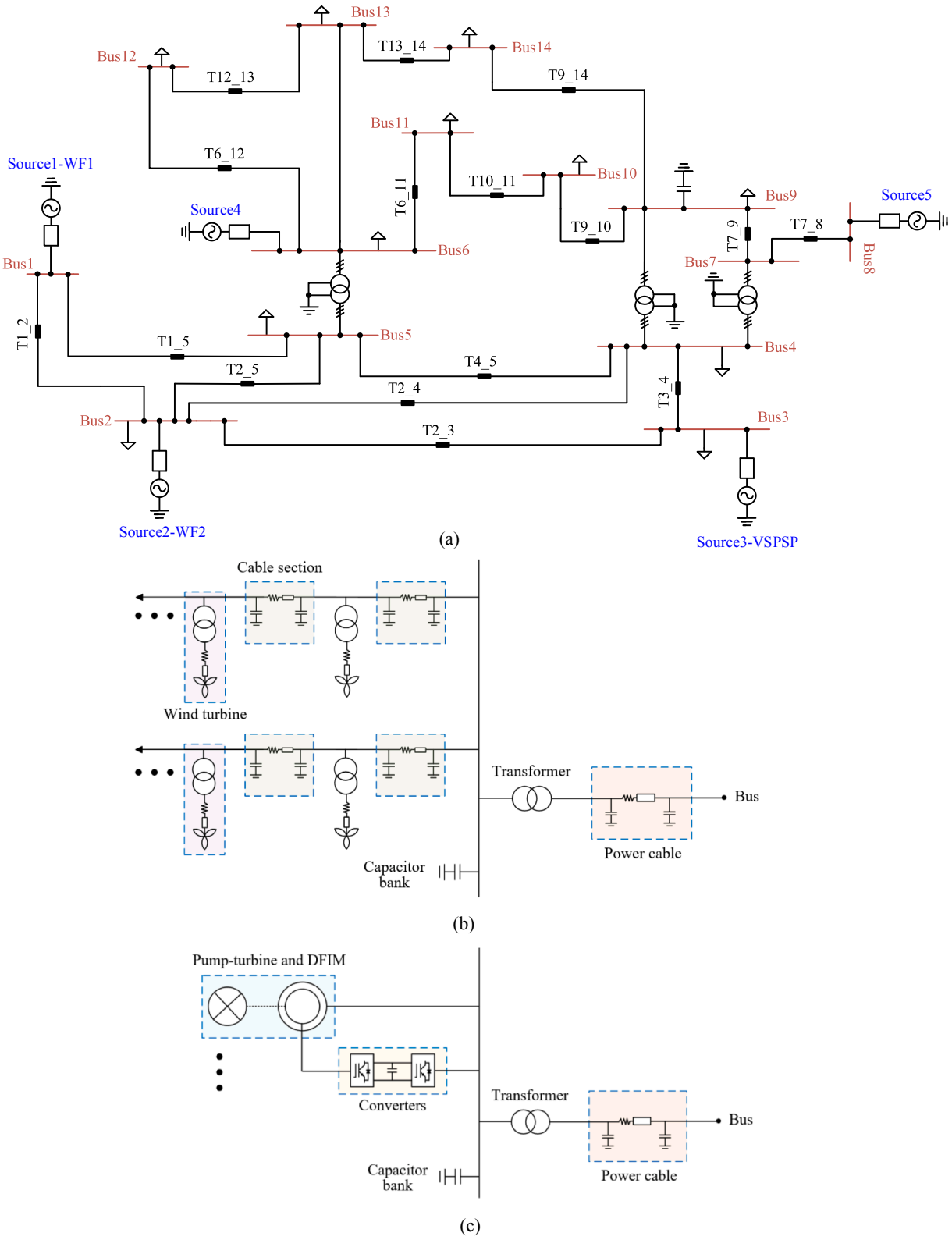

Fig. 10. The studied 14-bus isolated power system. (a) The model of the test system. (b) The diagram of wind farm. (c) The diagram of variable-speed pumped-storage.

input power and the static head variations [25]. This control principle can be described as

$$\frac{dy}{dt} = \frac{1}{T_y}\left(y_{ref} - y\right) \tag{21}$$

3.3. Vector control for the grid-side converter

The grid-side converter (GSC) is responsible for stabilizing the DC-bus voltage and regulating the power factor as shown in Fig. 6. To

Table 3
The active power share of each load.

Bus number	Power share (%)	Bus number	Power share (%)	Bus number	Power share (%)
2	7.97	6	4.11	12	2.24
3	34.58	9	10.83	13	4.96
4	17.55	10	3.30	14	5.47
5	2.79	11	1.28		

Table 4
References for three types of wind power.

Wind power references	Description	
Random wind (Gaussian)	**R1:**	**Frequency: 1.0 Hz; Mean value: 15 m/s; Standard deviation: 1.5**
	R2:	Frequency: 1.0 Hz; Mean value: 15 m/s; Standard deviation: 0.5
	R3:	Frequency: 0.05 Hz; Mean value: 20 m/s; Standard deviation: 0.5
	R4:	Frequency: 1.0 Hz; Mean value: 10 m/s; Standard deviation: 1.5
Gusty wind (sinusoidal)	**S1:**	**Frequency: 0.1 Hz; Amplitude: 2.5 m/s; Offset: 15 m/s**
	S2:	Frequency: 0.05 Hz; Amplitude: 2.5 m/s; Offset: 15 m/s
	S3:	Frequency: 0.1 Hz; Amplitude: 5 m/s; Offset: 15 m/s
Gradient wind (square)	**G1:**	**Frequency: 0.05 Hz; Initial amplitude: 10 m/s; Final amplitude: 20 m/s**
	G2:	Frequency: 0.05 Hz; Initial amplitude: 12.5 m/s; Final amplitude: 17.5 m/s
	G3:	Frequency: 0.1 Hz; Initial amplitude: 12.5 m/s; Final amplitude: 17.5 m/s

realize the independent control for the DC-bus voltage and reactive power in the *dq* reference frame, adopting the grid voltage as the directional vector, the GSC vector control structure is generally devised as shown in Fig. 6 which is widely developed and used for renewable power generation systems [33].

As the output oriented vector control based on *d*-axis grid voltage, the references for the grid-side voltage in the *dq* frame can be described as

$$v_{gd} = -R_g i_{gd} - L_g \frac{di_{gd}}{dt} u_{gd} + \omega_g L_g i_{gq} + u_{gd}, \tag{22}$$

$$v_{gq} = -R_g i_{gq} - L_g \frac{di_{gd}}{dt} - \omega_g L_g i_{gq}. \tag{23}$$

3.4. Vector control for the rotor-side converter

The feature of VSUs in the pump mode should be noted that the rotor speed variation is essential to exceed the movement of guide vane opening, otherwise, the units will drop into the reverse flow region [25]. Therefore, to guarantee the reliable operation in any transient states, the vector control for the rotor-side system with a rapid regulation is responsible for regulating the rotor speed of the VSU in the pump mode (Fig. 7).

The rotor voltage references as the output of the stator voltage oriented vector control can be described as

$$u_{rd} = R_r i_{rd} + \sigma L_r \frac{di_{rd}}{dt} - \omega_{slip}\left(-\frac{L_m}{\omega_s L_s} U_s + \sigma L_r i_{rq} \right), \tag{24}$$

$$u_{rq} = R_r i_{rq} + \sigma L_r \frac{di_{rd}}{dt} + \omega_{slip} \sigma L_r i_{rd}. \tag{25}$$

4. Dynamic behaviors of VSUs for the power storage regulation: Simulation results and measurement data

The primary purpose of this section is to validate the model presented and analyze the transient dynamic behaviours of hydraulic-mechanical–electrical coupling system during power tracking storage. Power regulation processes of a VSPSP are simulated, and the results are compared to the measurement data obtained from [25,26].

An experimental investigation is performed with two elementary power command signals (step power signal (SPS); ramp power signal (RPS)) for the Ohkawachi VSPSP unit #4. The detailed information, as well as the basic parameters of this VSU, are shown in Appendix 1 (Table 7); the suitable operating regime data provided by the manufacturer are shown in Appendix 2 through Fig. 15, including optimum rotor speed (ORS) and optimum guide vane opening (OGVO). The RBIM interpolation results of ORS and OGVO for the entire pump operating region can be seen from in Fig. 8.

According to the operating adjustable range for this VSU [25], the upper and lower ORS and OGVO limits are set from 330 to 390 rpm and from 40 to 100% respectively, during the calculation process. It can be seen from the Fig. 8 that the interpolation surfaces are matching with the data (red curves) which illustrate that RBIM is an appropriate method for VSPSPs to calculate optimal references. Table 2 compares the measurement data and interpolation results with the field test signal of SPS and RPS. The interpolated outcomes are consistent with the on-site measurement data which is clearly presenting the high accuracy of the RBIM.

The input power command signals are shown in Fig. 9(a) where both signals initiate at $t = 5$ s with 246 MW input power. The setting slope of the RPS is 6.32 MW/s and the signal reaches the maximum input power of 400 MW at 29.37 s. The setting step power variation of the SPS is 78 MW (accounting 19.5% of the rated power input). Fig. 9(b) shows that in the entire RPS regulation process in which the system input power delay does not exceed 0.2 s. Besides, the SPS simulation result illustrates that the system input power can reach the step power target within 0.6 s. These studies demonstrate that the VSUs can regulate power rapidly and flexibly in the pumped storage mode.

With the change in the input power command signal at 5 s, the optimum references conveyed into the control system are suddenly increasing which in turns leading to the variation of the rotor speed and guide vane opening as indicated in Fig. 9(c) and (d, respectively). Caused by the similar control principle, the changing trend of the rotor speed and guide vane opening are analogous. Furthermore, as mentioned in Section 3, the variation of the rotor speed is generally designed to be faster than the guide vane opening in order to prevent the units from dropping into the reverse flow region. It appears in these figures that the time of the rotor speed entering the steady-state (16.31 s) is shorter than that of the guide vane opening (19.87 s).

Finally, the simulation matches the test data, especially for the system power input: the maximum deviations of both signals are less than 0.2%. Some slight differences are presented in the comparison of the rotor speed simulation and measurement data and a possible explanation for this phenomenon is that the feed-forward control is activated [25]. Moreover, in the initial guide vane opening increasing stage, both signals based on the measured data are fractionally more significant than the simulation results which are probably due to the unusual fast response of the guide vane (close to the limiting rate). It can be concluded that the model presented in this paper adequately simulates the dynamic process of VSPSPs for the power storage regulation.

5. Rapid power storage regulation response of VSPSPs: Mitigating variations in wind power generation

This section aims to assess the power storage regulation performance of VSUs during the process of mitigating variations in wind power generation in order to demonstrate the dynamic behaviors (power

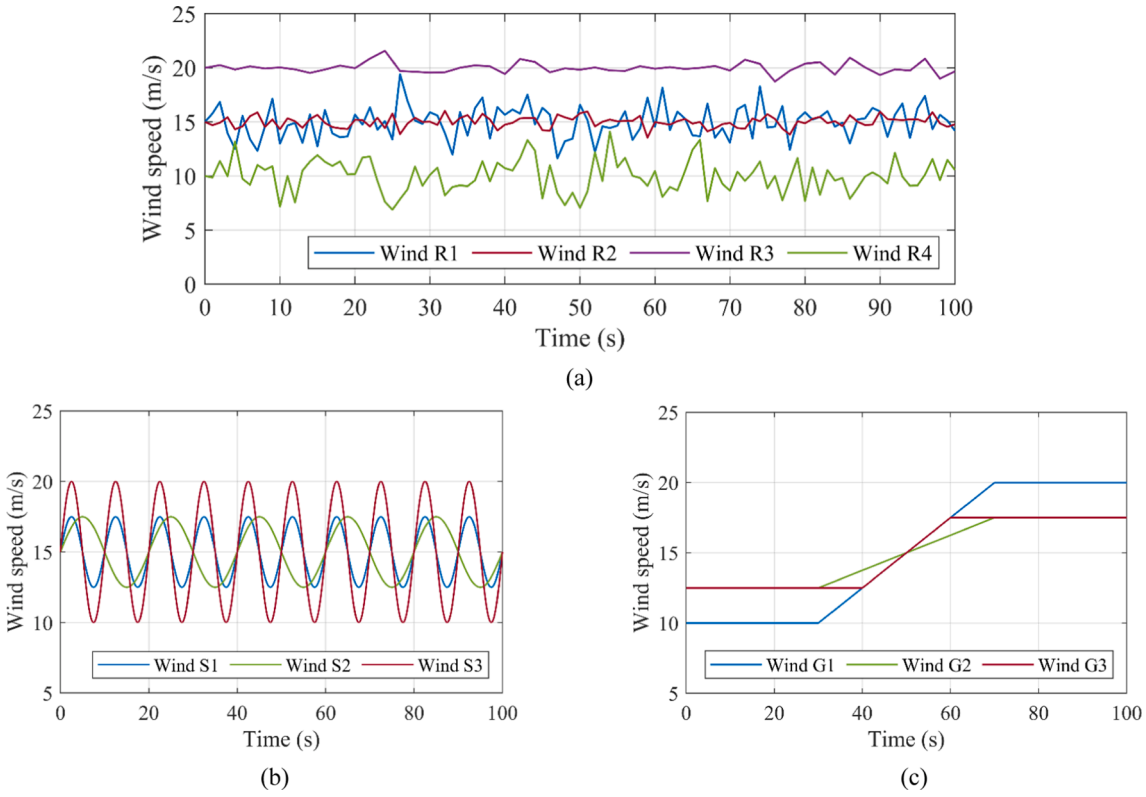

Fig. 11. Visual images of random, gradient and gusty winds applied in this study. (a) random winds (R1 to R4); (b) gusty winds (S1 to S3); (c) gradient winds (G1 to G3).

response and mechanical motion) of VSUs. To ensure the safety and stability of the hydraulic system during the transient process, studying the dynamic performance of the VSU under the power injection of time-varying wind energy becomes much more significant.

The description of the study cases is presented in Section 5.1 and the dynamic regulation performance of the VSU for mitigating the wind power variation is studied and analyzed in Section 5.2. Besides, assessments about the power regulation performance and changes in dynamic behaviors are conducted in Section 5.2 to contrast the regulation ability of PSPs in the power generation mode (VSUs and FSUs) and storage mode (VSUs).

5.1. Case descriptions

IEEE bus test systems are widely applied by researchers to implement new ideas and concepts in the research field of electrical power and energ system [38-42]. This paper focus on the regulation performance of VSU in mitigating the wind power variations, by appling IEEE 14-bus test system, the study cases are set as an isolated grid include different types of energy sources (wind, pumped-storage and conventional power) as shown in Fig. 10 (a). The power system is composed of 11 loads, 17 transmission lines and 5 electrical machines (marked as sources in figure), a one-line diagram to help understand the structure of the test system is presented in Fig. 16 in Appendix 3.

In this case study, the installed capacity of the two wind farms placed at buses 1 and 2 are 12 MW and 24 MW, respectively. The structure of the wind farms is presented in Fig. 10(b), it should be noticed that the selected wind turbine generators in this case study are doubly-fed asynchronous machines, i.e. DFIMs, and their modeling as well as operational principles can be found in [35]. VSUs applied in this test case and placed at Bus 3 are from an existing Chinese VSPSP in its feasibility study stage [24], the pumping power ranges within 8–12 MW, additional information of the units is presented in Table 7 (Appendix 1) and the values of parameters are shown in Table 9 (Appendix 1), the structure of which can be found in Fig. 10(b). The conventional energy sources placed at bus 6 and 8 are modeled as two synchronous generators, the nominal power of which are 10 MW and 15 MW, respectively. 11 of the 14 buses are set to be connected with load in the test system and the active power share of each load is shown in Table 3. The parameters of the transmission lines including impedance and length are presented in Table 10 in Appendix 3.

To study the performance of the power storage regulation for mitigating the wind power variations, three functions (Gaussian wave, sinusoidal wave and square wave functions) are applied to simulate the variation of the random, gusty and gradient wind speeds. The modeling of these wind speed types is presented in Appendix 4 and details of the different wind power references adopted in this section are listed in Table 4.

Four random winds profiles (R1, R2, R3 and R4) with different frequency, mean values and standard deviation; three gradient winds (G1, G2 and G3) and three gusty wind (S1, S2 and S3) are simulated. The diagram of these wind sequences is shown in Fig. 11.

5.2. Performance assessment during the mitigation of wind power variations

The objective of studying the power storage regulation is to reduce wind power curtailment and ensure a steady power supply. Taking the power references with random wind speed type as an example, this subsection presents the results of VSU for mitigating the wind power variations, Fig. 12 illustrates the regulation behaviors of the VSU under the influence of random winds.

For winds R2 and R3, it can be concluded from Fig. 12(b) and (c) that the power variation of the VSPSP input almost matches with the wind farm generation, i.e. providing a steady power supply and effectively alleviating the impacts on system frequency of random wind disturbances (the deviation of system frequency for both winds is less than 0.05%). Regarding the winds R1 and R4, it can be observed that the VSU

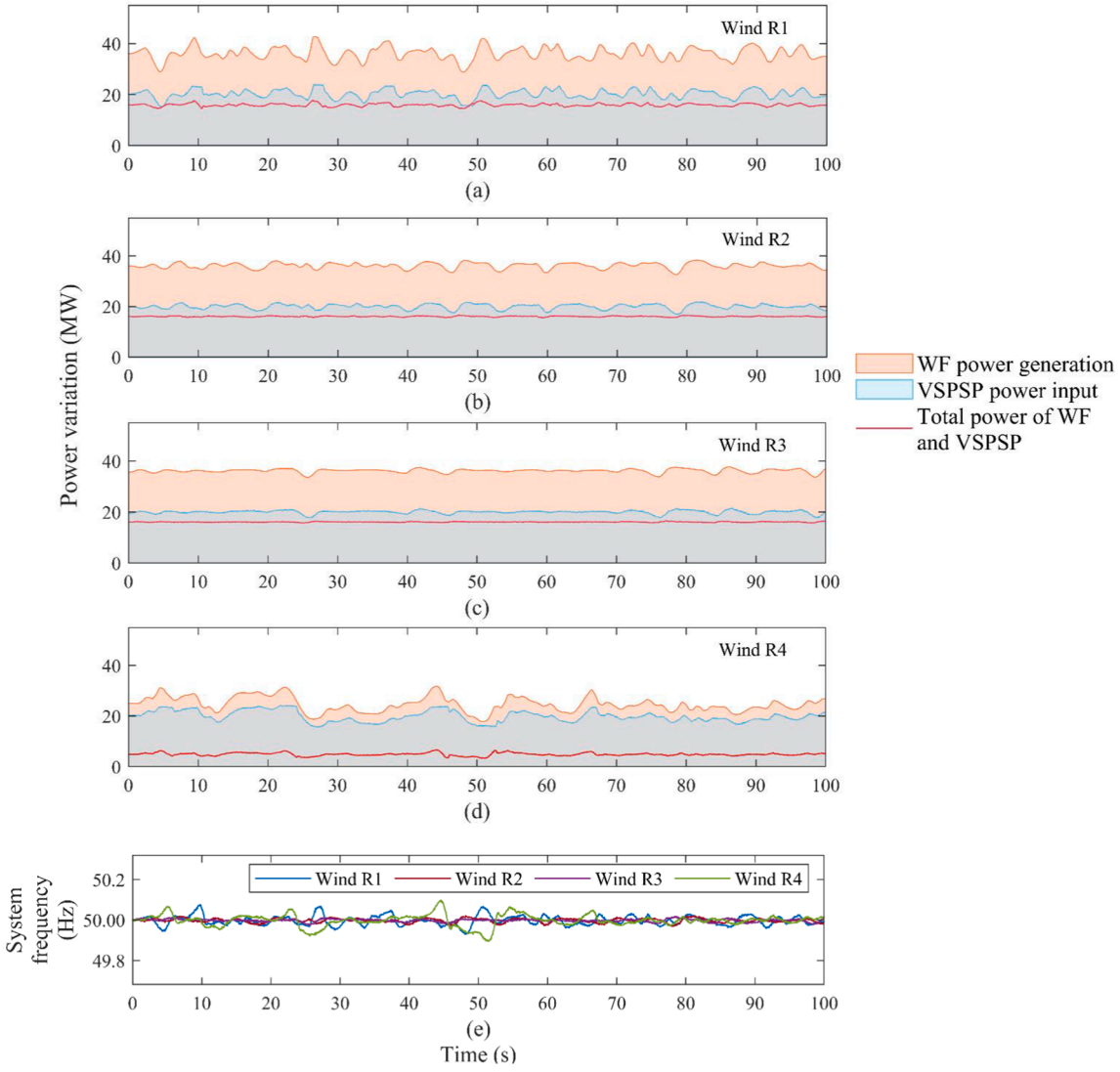

Fig. 12. Power and frequency responses with random wind disturbances (R1 to R4). (a), (b), (c) and (d). Power responses of WF and VSPSP. The wind farm power generation and VSPSP input power are shown in orange and blue areas respectively, while the red curves represent the total power. (e) Frequency responses of the test system.

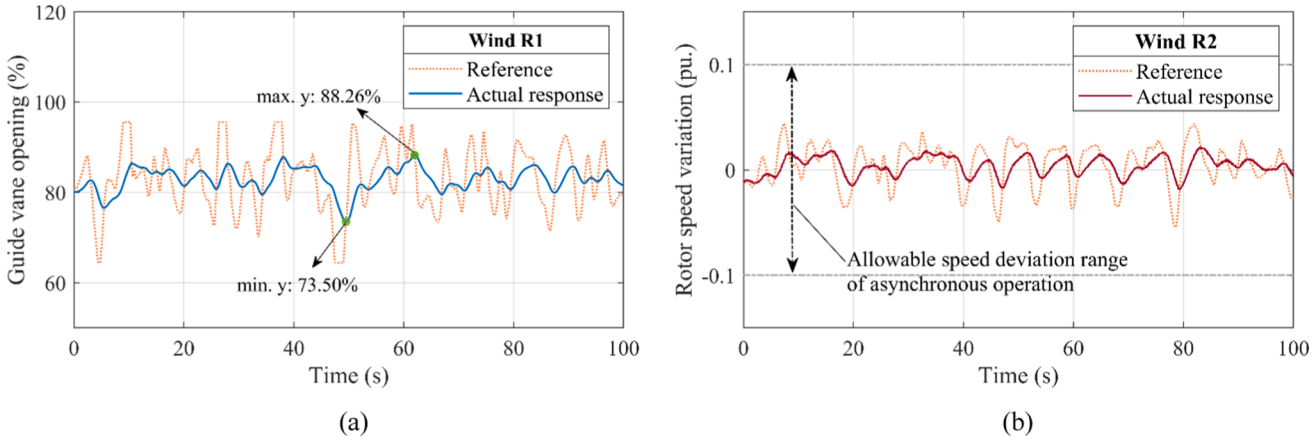

Fig. 13. Variation of the VSU guide vane and rotor speed influenced by random winds: (a) guide vane optimum reference and response with wind R1; (b) rotor speed optimum reference and response with wind R2.

Table 5
Regulation performance and dynamic behaviors of VSU for mitigating wind power variations.

Wind power		Power differences (MW)		Guide vane opening (%)		Rotor speed (pu.)	
Type	Item	STD	Range	STD	Range	STD	Range
Random	R1	0.5565	3.4635	2.7312	14.7781	2.12E-02	1.17E-01
	R2	0.1807	1.3987	1.1901	5.1003	9.03E-03	3.91E-02
	R3	0.1595	1.0759	1.0657	4.7740	7.70E-03	3.60E-02
	R4	0.5730	3.4379	3.2019	16.2163	2.33E-02	1.43E-01
Gusty	S1	0.7633	4.2815	6.0721	27.8181	4.31E-02	1.67E-01
	S2	0.2276	1.6698	4.2152	14.0340	2.58E-02	1.06E-01
	S3	3.0683	7.4262	11.7371	35.1127	4.81E-02	1.97E-01
Gradient	G1	0.2091	1.1375	1.9544	6.7598	1.48E-02	4.07E-02
	G2	0.1765	0.8799	0.9815	3.2371	6.70E-03	2.07E-02
	G3	0.1863	1.0654	1.3546	5.0762	7.78E-03	3.06E-02

1. "STD" means standard deviation.
2. "Range" represent the difference of maximum and minimum values here.

1. "STD" means standard deviation.
2. "Range" represent the difference of maximum and minimum values here.

Table 6
Regulation time delay of PSPs in different operational states.

The type and operation state of PSPs	Regulation time delay (s)									
	Random winds				Gusty winds			Gradient winds		
	R1	R2	R3	R4	S1	S2	S3	G1	G2	G3
VSU in storage mode	0.27	0.19	0.18	0.29	0.36	0.19	0.28	0.15	0.13	0.12
VSU in generation mode	0.27	0.19	0.18	0.29	0.36	0.19	0.28	0.15	0.13	0.12
FSU in generation mode	3.76	2.92	2.79	3.81	3.93	2.95	2.72	2.63	2.40	2.57

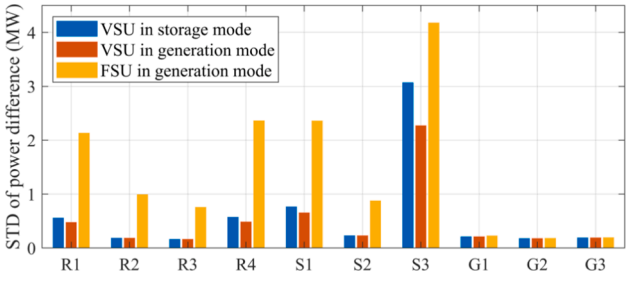

Fig. 14. The standard deviation of power differences results.

maintains at a fixed-power-input (maximum or minimum power input) operating state instead of tracking the wind power variations during some periods (such as 8.98–10.52 s of wind R1 and 4.21–5.85 s of wind R4) which result in the substantial fluctuations of system frequency as presented in Fig. 12(e). The phenomenon is due to the drastic variations of the wind power generation that lead to the instant power storage demand out of the VSU adjustable range. Compared the results with winds R1 and R2, this is attributed to a lower standard deviation of the wind speed (0.5 vs 1.5).

The mechanical dynamic behaviors (guide vane opening and rotor speed) of the VSU with random wind disturbance are presented in Fig. 13. It can be concluded that owing to the apparently longer time required for mechanical motion compared with that of electrical response, differences are presented between the reference settings and actual responses which are exhibiting lags in the time-domain. However, time lags are beneficial to mitigate the fluctuations of guide vane opening and rotor speed variations, thereby, promoting the stability of the system during the regulation process.

The model outcomes of the regulation performances and dynamic behaviors are presented in Table 5 under the variation of the three tested wind speed. As a result of the relatively large standard deviation of wind speeds, the STD and range of the power difference for the R1 and R4 wind-profiles seem to be greater than that for R2 and R3 (over 3 times for STD and over 2 times for the range). Thus, the regulation performance for wind power references of R2 and R3 performs better than that of R1 and R4 which is actually consistent with the results obtained in Fig. 12. Due to the substantial variations of the wind speed of S3 (the largest variation in the amplitude is tested) that leads in high and frequent power injections above the adjustable range of VSUs, the regulation performance is unsatisfied and the power differences appear to be larger than other wind sequences. Besides, from the comparison of the results of S2 and S3, it can be drawn that a low frequency for gusty wind is of great benefit for the improvement of the power regulation performance. Regarding the gradient wind speeds, the VSU performs excellently and the power supplies are the most stable for all the wind speed types. Moreover, it can be also concluded from Table 5 that the fluctuation degrees in the dynamic behaviors of the VSU for the winds

R2 and R3 are much smaller than that for R1 and R4 wind profiles which are showing potential for improving the stability of VSUs under the lower wind speed deviation.

6. Comparison of the power regulation quality: pumped-storage mode vs power generation mode

In the previous sections, the VSU in the pumping mode is proved to effectively mitigate the impact of wind power variations on the electricity supply. From the aspects of the power regulation quality, this section focuses on the comparison of the PSP's regulation performance in the storage mode (only for VSU) and generation mode (for both FSU and VSU).

When evaluating the regulation quality of the electrical equipment, the response time and power regulation differences are two common and critical indicators which are widely applied and studied in [36,37]. Additionally, these two indicators are generally related. A faster response promotes smaller power differences and longer delays commonly result in unsatisfied regulation performance with substantial power fluctuations. The test results based on these two indicators under all ten sequences of wind power references (i.e., R1 to R4, S1 to S3, and G1 to G3) are compared for the power storage mode (VSU) and generation mode (VSU and conventional FSU) in Table 6 and Fig. 14.

The regulation time delay (RTD) results of the VSU in the pumped-storage mode are entirely consistent with the hydro-turbine mode as a result of applying the same operational power adjustment control approach (vector control). Theoretically, the alike response time should lead to equal power regulation results (power differences) and yet, it can be drawn from Fig. 14 that for the two operational modes of the VSU, partial results of the power differences (R1, R4, S1 and S3) are distinct and power generation mode perform better. The reason for this is that the operational power adjustable range of the generation mode is generally larger than that of the storage mode (6 MW for the generation mode and 4 MW for the storage mode in this case) which is promoting the generation mode of VSUs for handling a wider range of wind power fluctuations.

Regarding the comparison of the VSU and FSU as the electrical reaction in VSUs is extremely faster than mechanical motion (namely the power consumption adjustment for FSUs), the power tracking response delay for the variable-speed operation is significantly smaller than the fixed-speed operation for all wind sequences. The RTD ratios of VSUs to FSUs range between 4.67 and 9.16%, demonstrating the rapidity of VSPSPs in the power regulation. As mentioned before, the results of the power difference and time regulation delay are generally relevant. Fig. 15 shows that the results of the power difference for random and gusty winds with the FSU are much larger than that of the VSU due to the longer regulation time delay. For random winds, the ratios (STD of the power difference) of the VSU in the power storage to the FSU in the power generation are within the range of 18.30–26.12% and the outcomes for gusty winds (i.e., S1, S2, and S3) are 32.38%, 26.07%, and 73.49%, respectively. The ratio for S3 overpasses other winds as the power storage demand exceeds the power input adjustable range in 78.9% of the time and leading to the rapid power regulation of VSUs which does not produce a significant effect. Additionally, for gradient winds, although the apparent differences are still presented in the regulation time delay results, the power differences results are almost similar (the results of the VSU account for 93.72–98.03% that of the FSU). This phenomenon demonstrates that comparing with the random and gusty winds, the variation trends of gradient winds are relatively simple which is making the power regulation task less difficult and the results in the power difference are insensitive to the time delay.

7. Conclusions

In this study, a short-term dynamic analysis with a timescale of seconds on VSPSPs for mitigating the wind power variation is conducted based on the IEEE 14-bus test system. The main focus is the assessment of the power storage regulation quality for VSUs under different wind scenarios, which is a key characteristic in terms of the contribution to the integration of renewable energy systems. Another major contribution is the comparison of the regulation quality between VSUs under the pumped-storage mode with other operational states of PSPs which provide effective guidance for the power system regulation arrangements. Firstly, a model integrating hydraulic-mechanical–electrical subsystems of VSPSPs with DFIMs is developed and based on radial basis interpolation method, a novel calculation approach is proposed for optimum operational references. According to the Ohkawachi VSPSP, the dynamic processes during the power storage regulation of VSPSPs are simulated and compared with on-site measurements. It has been proved that the proposed model and the calculation method for optimum references can be an effective tool for further investigations on the performance evaluation and parameter tuning of VSPSPs. Secondly, by considering different wind scenarios (random, gradient, and wind gust speeds), the dynamic process of the VSU in mitigating the wind power variations are simulated. The simulations results reveal that the rapid adjustable operational power enables VSUs to effectively and promptly alleviate the impacts of the intermittent wind power generation variations on electricity supply. Interestingly, the quality of the regulation for VSUs is closely relevant to the random wind speed standard deviation as well as to the frequency of the gusty wind speed. Conversely, there is a weak sensitivity of the VSU's regulation to the gradient wind speeds.

Finally, two widely applied and extremely significant power regulation evaluation indicators are adopted to compare the regulation quality of VSPSPs in the pumping mode with other operating conditions. The results demonstrate that both storage and generation modes of VSUs possess an excellent regulation ability except for the power-adjustable range in the generation mode. Actually, for the studied case, the power-adjustable range of the pumped-storage operation is 33.3% less than that of the hydro-turbine operation. Besides, due to the apparent longer time delay of the mechanical motion (FSU) compared with that of electrical response (VSU), the regulation performance of the VSU (both generation and storage modes) is better than that of the FSU (generation mode), especially in the aspect of dealing with wind speeds with frequent power variations (random and gusty winds). Specifically, for all wind power references applied in this work, the regulation time delays of FSUs are more than twelve times larger than that of VSUs and for most random and gusty wind profiles, the standard deviation of the power regulation difference of VSU is less than 35% of the FSU. The results for the test cases demonstrate that the VSU in the pumping mode is more suitable and reliable for undertaking the task of mitigating the wind power variations compared with that of conventional hydraulic equipment.

CRediT authorship contribution statement

Yuwen Deng: Conceptualization, Software, Methodology. **Pengfei Wang:** Data curation, Methodology. **Alessandro Morabito:** Validation. **Wenfeng Feng:** Visualization, Investigation. **Apel Mahmud:** Validation. **Diyi Chen:** Supervision. **Patrick Hendrick:** Supervision.

Declaration of Competing Interest

The authors declare that they have no known competing financial

interests or personal relationships that could have appeared to influence the work reported in this paper.

Acknowledgements

This research is supported by the scientific research foundation of the Natural Science Foundation of Shaanxi Province of China (2019JLP-24), Shaanxi Science and Technology Innovation Team, and Water Conservancy Science and Technology Program of Shaanxi Province (2018slkj-9).

Appendix

1. Values of different parameters for the pump-turbine units.

See Tables 7–9.

Table 7
Basic parameters of the Ohkawachi VSPSP unit #4 (VSU 1) and a Chinese VSPSP (VSU 2).

Item	Synchronousspeed	Maximum power output	Power input adjustable range	Number of pole pairs	Rated grid frequency
VSU1	360 rpm	320 MW	240–400 MW	10	60 HZ
VSU2	500 rpm	10 MW	8–12 MW	6	50 HZ

Table 8
Values of the parameters for VSU 1.

DFIM		Pump-turbine		Waterway and governor		Controllers	
Para.	Values	Para.	Values	Para.	Values	Para.	Values
T_a	11.0 s	e_y	0.95 pu.	T_r	1.20 s	K_p (GVC)	0.12
L_s	3.60 pu.	e_ω	−0.75 pu.	T_w	1.52 s	K_i (GVC)	11.00
L_r	3.60 pu.	e_h	1.50 pu.	T_y	0.45 s	K_p (RVC)	0.10
R_s	0.012 pu.	e_{qy}	0.65 pu.	T_a	0.90 s	K_i (RVC)	10.10
R_r	0.013 pu.	$e_{q\omega}$	0.10 pu.	/	/	/	/
L_m	3.48 pu.	e_{qh}	0.47 pu.	/	/	/	/

I. “GVC” represent the grid-side vector control.
II. “RVC” represent the rotor-side vector control.

Table 9
Values of the parameters for VSU 2.

DFIM		Pump-turbine		Waterway and governor		Controllers	
Para.	Values	Para.	Values	Para.	Values	Para.	Values
T_a	10.0 s	e_y	0.95 pu.	T_r	0.36 s	K_p (GVC)	0.10
L_s	1.32 pu.	e_ω	−0.75 pu.	T_w	1.55 s	K_i (GVC)	12.00
L_r	1.36 pu.	e_h	1.50 pu.	T_y	0.45 s	K_p (RVC)	0.10
R_s	0.0045 pu.	e_{qy}	0.65 pu.	T_a	0.90 s	K_i (RVC)	11.50
R_r	0.0022 pu.	$e_{q\omega}$	0.10 pu.	/	/	/	/
L_m	1.23 pu.	e_{qh}	0.47 pu.	/	/	/	/

I. “GVC” represent the grid-side vector control.
II. “RVC” represent the rotor-side vector control.

2. Operational characteristic curves of Ohkawachi PSP unit #4 [25].

See Fig. 15.
The variable speed pumped storage unit commissioned on the 3rd December 1993, the speed adjustable range is set as 330–390 rpm and the maximum power input is 400 MW. The lowest operational water head is around 353 m and the highest head is around 421 m.

3. Supplementary information of the test system.
I. One-line diagram of the test system

One-line diagrams are widely applied in the research field of electrical power and energy system to help the readers understand the structure of the grid [41], the diagram of the test system in this paper is presented in Fig. 16.

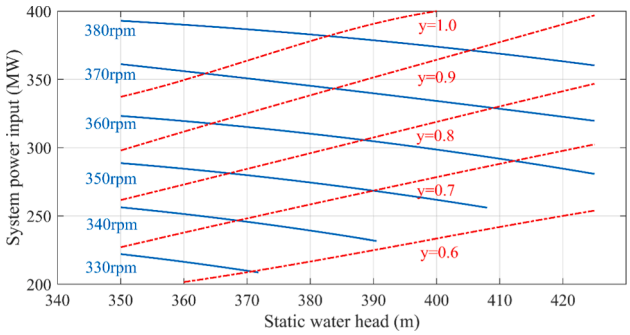

Fig.15. Pump mode optimum references curves provided by the manufacturer.

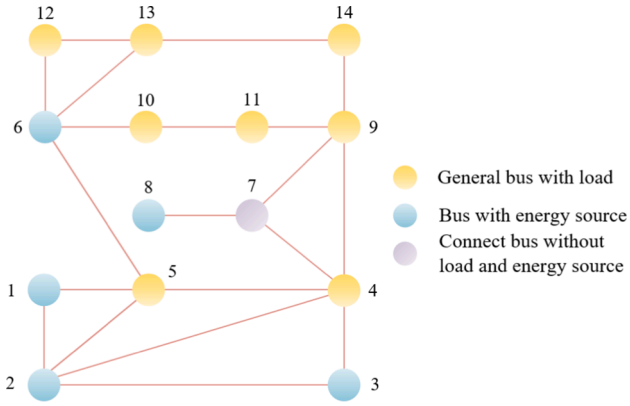

Fig. 16. One-line diagram of the test system in this paper.

II. Test system in simulation tools

Based on the simulation platform of Matlab/Simulink, the test system is built and can be presented in Fig. 17.

III. Transmission line parameters

The transmission lines in the test system of this paper are modelled applying the Bergeron model. According to the typical line reactance values,

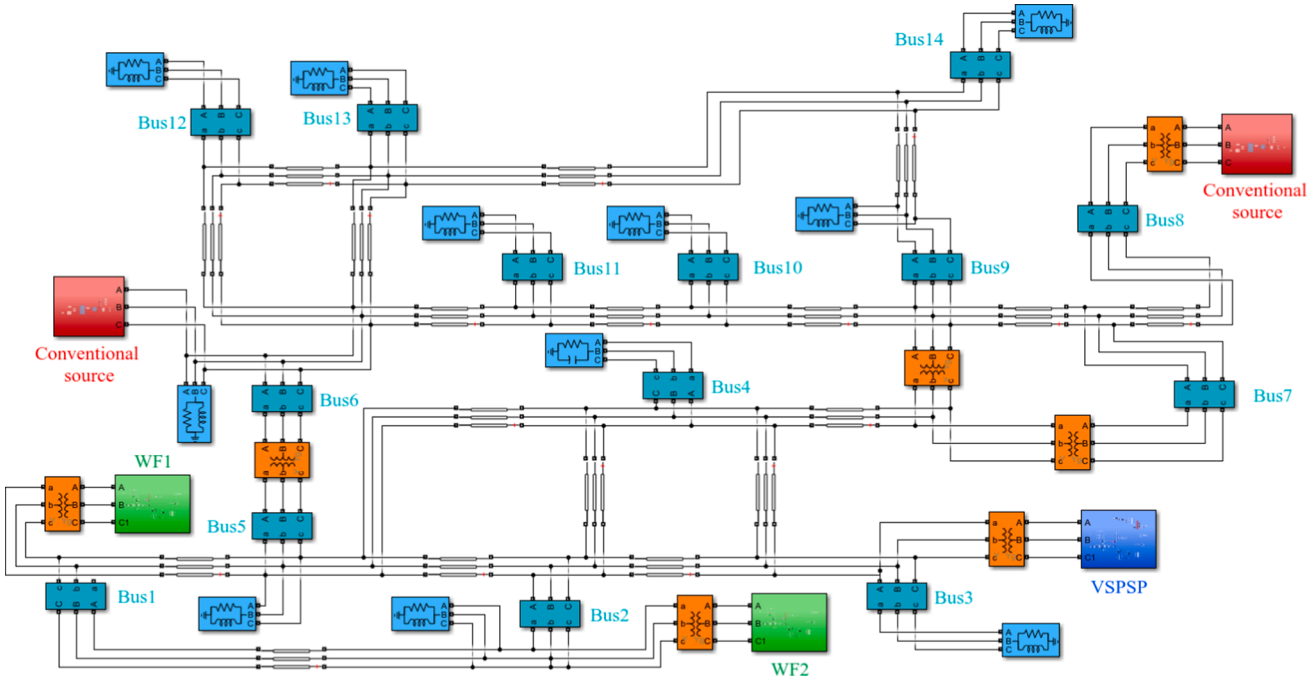

Fig. 17. The studied IEEE-14 bus system model in Simulink.

Table 10
Transmission line parameters.

From Bus	To Bus	Resistance-R (Ω)	Reactance-X (Ω)	Length of the line (km)
1	2	9.23E+00	1.13E+01	2.25E+01
1	5	7.64E+00	4.25E+01	8.49E+01
2	3	1.06E+01	3.77E+01	7.54E+01
2	4	9.38E+00	3.35E+01	6.70E+01
2	5	9.28E+00	3.31E+01	6.63E+01
3	4	9.11E+00	3.26E+01	6.51E+01
4	5	6.56E+00	8.02E+00	1.60E+01
6	11	1.06E+01	3.79E+01	7.58E+01
6	12	8.78E+00	4.88E+01	9.75E+01
6	13	2.03E+01	2.48E+01	4.95E+01
7	8	9.38 E+00	3.35E+01	6.70E+01
7	9	1.72E+01	2.09E+01	4.19E+01
9	10	1.32E+01	1.61E+01	3.22E+01
9	14	4.22E+00	5.14E+01	1.03E+01
10	11	1.02E+01	3.66E+01	7.31E+01
12	13	1.07E+01	3.81E+01	7.62E+01
13	14	11.97E+00	6.63E+01	1.33E+02

Table 10t summarizes the transmission line parameters.

The mathematical modelling of wind speeds

This paper considers three types of wind speeds which are random, gusty, and gradient winds. The main content of this section is to describe the mathematical model of these wind speeds. Another table is in the following to explain the meanings of different parameters and variables used in this part.

Nomenclature for Appendix 4

Parameters, Variables

φ	stochastic variable (pu.)
ω	wind speed frequency spacing (HZ)
μ	the average wind speed (m/s)
F	the disturbance range (pu.)
K_N	surface roughness factor (pu.)
T_{gd}	duration of gradient wind (s)
T_{gs}	start time of gradient wind (s)
T_{sd}	duration of gusty wind (s)
T_{se}	end time of gusty wind (s)
T_{ss}	start time of gusty wind (s)
V_g	gradient wind speed (m/s)
V_r	random wind speed (m/s)
V_s	gusty wind speed (m/s)

Subscripts, Superscripts

i	iterative number between 1 and N
max	the maximum values

I. Random winds

The Gaussian noise is usually used to describe the behavior of random winds, the expression of random winds are

$$V_r = 2\sum_{i=1}^{N}(S_R(\omega_i)\Delta\omega)^{\frac{1}{2}}cos(\omega_i+\varphi_i), \tag{A.1}$$

$$\omega_i = (i-0.5)\Delta\omega, \tag{A.2}$$

$$S_R(\omega_i) = \frac{2K_NF^2|\omega_i|}{\pi^2[1+(\frac{F\omega_i}{\mu\pi})^2]^{\frac{3}{4}}}. \tag{A.3}$$

II. Gusty winds

The gusty winds reflects the sudden variation in the wind speed, and they are generally applied to indicate the large wind disturbances. It is generally described as

$$V_s = \begin{cases} 0, \ t < T_{ss} \\ \frac{V_{smax}}{2}[1-cos(2\pi\frac{t}{T_{sd}}-\frac{T_{ss}}{T_{sd}})], \ T_{ss}\leqslant t\leqslant T_{ss}+T_{sd} \\ 0, \ t > T_{ss}+T_{sd} \end{cases} \tag{A.4}$$

III. Gradient winds

The gradient winds are mainly applied to describe the gradual variation of wind speeds, the piecewise linearization modelling of which can be

described as

$$V_g = \begin{cases} 0, \ t < T_{gs} \\ V_{gmax}(1 - \dfrac{t - T_{gs}}{T_d}), \ T_{gs} \leqslant t < T_{gs} + T_{gd} \\ V_{gmax}, \ T_{gs} + T_{gd} \leqslant t < T_{ge} \\ 0, \ T_{ge} \leqslant t \end{cases} \tag{A.5}$$

References

[1] Elliott D. A balancing act for renewables. Nat Energy 2016;1:15003.
[2] Chang MK, Eichman JD, Mueller F, Samuelsen S. Buffering intermittent renewable power with hydroelectric generation: a case study in California. Appl Energy 2013; 112:1–11.
[3] Pérez-Díaz JI, Chazarra M, García-González J, Cavazzini G, Stoppato A. Trends and challenges in the operation of pumped-storage hydropower plants. Renew Sustain Energy Rev 2015;44:767–84.
[4] Kocaman AS, Modi V. Value of pumped hydro storage in a hybrid energy generation and allocation system. Appl Energy 2017;205:1202–15.
[5] Murage MW, Anderson CL. Contribution of pumped hydro storage to integration of wind power in Kenya: An optimal control approach. Renew Energy 2014;63: 698–707.
[6] Bhayo BA, Al-Kayiem HH, Gilani SIU, Ismail FB. Power management optimization of hybrid solar photovoltaic-battery integrated with pumped-hydro-storage system for standalone electricity generation. Energy Convers Manage 2020;215.
[7] Levieux LI, Inthamoussou FA, De Battista H. Power dispatch assessment of a wind farm and a hydropower plant: A case study in Argentina. Energy Convers Manage 2019;180:391–400.
[8] Kaldellis JK, Kapsali M, Kavadias KA. Energy balance analysis of wind-based pumped hydro storage systems in remote island electrical networks. Appl Energy 2010;87(8):2427–37.
[9] Zhang Y, Ma C, Lian J, Pang X, Qiao Y, Chaima E. Optimal photovoltaic capacity of large-scale hydro-photovoltaic complementary systems considering electricity delivery demand and reservoir characteristics. Energy Convers Manage 2019;195: 597–608.
[10] Ma T, Yang H, Lu L, Peng J. Pumped storage-based standalone photovoltaic power generation system: modeling and techno-economic optimization. Appl Energy 2015;137:649–59.
[11] Tang Y, Fang G, Tan Q, Wen X, Lei X, Ding Z. Optimizing the sizes of wind and photovoltaic power plants integrated into a hydropower station based on power output complementarity. Energy Convers Manage 2020;206.
[12] Bhandari B, Poudel SR, Lee K-T, Ahn S-H. Mathematical modeling of hybrid renewable energy system: a review on small hydro-solar-wind power generation. Int J Prec Eng Manuf-Green Technol 2014;1(2):157–73.
[13] Soukissian T. Use of multi-parameter distributions for offshore wind speed modeling: The Johnson S-B distribution. Appl Energy 2013;111:982–1000.
[14] Li D, Yan W, Li W, Ren Z. A Two-Tier Wind Power Time Series Model Considering Day-to-Day Weather Transition and Intraday Wind Power Fluctuations. IEEE T Power Syst 2016;31(6):4330–9.
[15] Zakeri B, Syri S. Electrical energy storage systems: A comparative life cycle cost analysis. Renew Sustain Energy Rev 2015;42:569–96.
[16] Varkani AK, Daraeepour A, Monsef H. A new self-scheduling strategy for integrated operation of wind and pumped-storage power plants in power markets. Appl Energy 2011;88(12):5002–12.
[17] Amirante R, Cassone E, Distaso E, Tamburrano P. Overview on recent developments in energy storage: Mechanical, electrochemical and hydrogen technologies. Energy Convers Manage 2017;132:372–87.
[18] Li DY, Zuo ZG, Wang HJ, Liu SH, Wei XZ, Qin DQ. Review of positive slopes on pump performance characteristics of pump-turbines. Renew Sustain Energy Rev 2014;31:746–61.
[19] Sivakumar N, Das D, Padhy NP. Variable speed operation of reversible pump-turbines at Kadamparai pumped storage plant - A case study. Energy Convers Manage 2014;78:96–104.
[20] Deane JP, Ó Gallachóir BP, McKeogh EJ. Techno-economic review of existing and new pumped hydro energy storage plant. Renew Sustain Energy Rev 2010;14(4): 1293–302.
[21] Feng C, Li C, Chang Li, Ding T, Mai Z. Advantage analysis of variable-speed pumped storage units in renewable energy power grid: Mechanism of avoiding S-shaped region. Int J Elec Power 2020;120.
[22] Iliev I, Trivedi C, Dahlhaug OG. Variable-speed operation of Francis turbines: A review of the perspectives and challenges. Renew Sustain Energy Rev 2019;103: 109–21.
[23] Koritarov V, Veselka TD, Gasper J, Bethke BM, Botterud A, Wang J, et al. Modeling and analysis of value of advanced pumped storage hydropower in the United States. Argonne Natl Lab (ANL); 2014.
[24] Yang W, Yang J. Advantage of variable-speed pumped storage plants for mitigating wind power variations: Integrated modelling and performance assessment. Appl Energy 2019;237:720–32.
[25] Kuwabara T, Shibuya A, Furuta H, Kita E, Mitsuhashi K. Design and dynamic response characteristics of 400 MW adjustable speed pumped storage unit for Ohkawachi Power Station. IEEE T Energy Conver 1996;11(2):376–84.
[26] Lung J-K, Lu Y, Hung W-L, Kao W-S. Modeling and dynamic simulations of doubly fed adjustable-speed pumped storage units. IEEE T Energy Conver 2007;22(2): 250–8.
[27] Koritarov V, Guzowski L, Feltes J, Kazachkov Y, Gong B, Trouille B, et al. Modeling adjustable speed pumped storage hydro units employing doubly-fed induction machines. Argonne National Laboratory; 2013.
[28] Muljadi E, Singh M, Gevorgian V, Mohanpurkar M, Hovsapian R, Koritarov V. Dynamic modeling of adjustable-speed pumped storage hydropower plant. IEEE PES general meeting. Denver, CO, USA. 2015.
[29] Louvet R, Neto A, Billet L, Passelergue J. Smart dispatch of variable-speed Pump Storage Plants to facilitate the insertion of intermittent generation. Paris (France): Cigré Session; 2016.
[30] Suul JA, Uhlen K, Undeland T. Wind power integration in isolated grids enabled by variable speed pumped storage hydropower plant. In: IEEE international conference on sustainable energy technologies. Singapore, Singapore; 2009. p. 399–404.
[31] Belhadji L, Bacha S, Munteanu I, Rumeau A, Roye D. Adaptive MPPT applied to variable-speed microhydropower plant. IEEE T Energy Conver 2013;28(1):34–43.
[32] Li H, Xu B, Mahmud MA, Chen D, Zhang J. Pumping phase modulation analysis for operational quality of a pumped-storage generating system. Energy Convers Manage 2019;199.
[33] Kim J, Muljadi E, Gevorgian V, Mohanpurkar M, Luo Y, Hovsapian R, et al. Capability-coordinated frequency control scheme of a virtual power plant with renewable energy sources. IET Gener Trans Dis. 2019;13(16):3642–8.
[34] Maisonnave O, Moreau L, Aubrée R, Benkhoris M-F, Neu T, Guyomarc'h D. Optimal energy management of an underwater compressed air energy storage station using pumping systems. Energy Convers Manage 2018;165:771–82.
[35] Kheshti M, Ding L, Bao W, Yin M, Wu Q, Terzija V. Toward intelligent inertial frequency participation of wind farms for the grid frequency control. IEEE T Iin Inform 2020;16(11):6772–86.
[36] Munoz-Hernandez GA, Mansoor SAP, Jones DI. Modelling and controlling hydro-power plants. London: Springer; 2013.
[37] Yang W, Yang J, Guo W, Norrlund P. Response time for primary frequency control of hydroelectric generating unit. Int J Electr Power Energy Syst 2016;74:16–24.
[38] Aljarrah R, Marzooghi H, Yu J, Terzija V. Sensitivity analysis of transient short circuit current response to the penetration level of non-synchronous generation. Int J Electr Power Energy Syst 2021;125:106556. https://doi.org/10.1016/j.ijepes.2020.106556.
[39] Ding L, Gonzalez-Longatt FM, Wall P, Terzija V. Two-step spectral clustering controlled islanding algorithm. IEEE T Power Syst 2013;28(1):75–84.
[40] Nazari-Heris F, Mohammadi-ivatloo B, Nazarpour D. Network constrained economic dispatch of renewable energy and CHP based microgrids. Int J Electr Power Energy Syst 2019;110:144–60.
[41] Mallick S, Rajan DV, Thakur SS, Acharjee P, Ghoshal SP. Development of a new algorithm for power flow analysis. Int J Electr Power Energy Syst 2011;33(8): 1479–88.
[42] Vaccaro A, Loia V, Formato G, Wall P, Terzija V. A self-organizing architecture for decentralized smart microgrids synchronization, control, and monitoring. IEEE T Ind Inform 2015;11(1):289–98.